Enhanced Spontaneous Skin Tumorigenesis and Aberrant Inflammatory Response to UVB Exposure in Immunosuppressed Human Papillomavirus Type 8–Transgenic Mice

Cinzia Borgogna[1], Licia Martuscelli[1], Carlotta Olivero[2], Irene Lo Cigno[1], Marco De Andrea[3,4], Valeria Caneparo[1,4], Renzo Boldorini[5], Girish Patel[2] and Marisa Gariglio[1,4]

Human papillomaviruses (HPVs) from the beta genus are commensal viruses of the skin usually associated with asymptomatic infection in the general population. However, in individuals with specific genetic backgrounds, such as patients with epidermodysplasia verruciformis, or those with immune defects, such as organ transplant recipients, they are functionally involved in sunlight-induced skin cancer development, mainly keratinocyte carcinoma. Despite their well-established protumorigenic role, the cooperation between β-HPV infection, impaired host immunosurveillance, and UVB exposure has never been formally shown in animal models. In this study, by crossing skin-specific HPV8-transgenic mice with *Rag2*-deficient mice, we have generated a preclinical mouse model, named *Rag2*$^{-/-}$:K14-HPV8. These mice display an unhealthy skin phenotype and spontaneously develop papilloma-like lesions spreading to the entire skin much more rapidly compared with *Rag2*$^{+/+}$:K14-HPV8 mice. Exposure to low doses of UVB radiation is sufficient to trigger severe skin inflammation in *Rag2*$^{-/-}$:K14-HPV8 but not in *Rag2*$^{+/+}$:K14-HPV8 mice. Their inflamed skin very much resembled that observed in cutaneous field cancerization in organ transplant recipients, showing high levels of UVB-damaged cells, enhanced production of proinflammatory cytokines, and mast cell recruitment to the dermis. Overall, this immunocompromised HPV8-transgenic mouse model shows that the coexistence of immune defects, β-HPV, and UVB exposure promotes skin cancer development.

Journal of Investigative Dermatology (2023) **143,** 740–750; doi:10.1016/j.jid.2022.10.023

INTRODUCTION

Human papillomaviruses (HPVs) are ubiquitous non-enveloped DNA viruses that specifically target keratinocytes residing in mucosal and skin sites (Kranjec and Doorbar, 2016; Lambert et al., 2020). To date, more than 220 HPV types have been completely sequenced and classified into five genera (McBride, 2022; Van Doorslaer et al., 2017), among which *Alphapapillomaviruses* (α-HPVs), such as HPV16 and 18, and *Betapapillomaviruses* (β-HPVs), such as HPV5 and 8, have been respectively linked to cancers at different anatomical sites (e.g., genital, skin and head and neck) (Galloway and Laimins, 2015; Kreuter et al., 2009; Lechner et al., 2022; Quint et al., 2015; Tetzlaff et al., 2019).

A large body of literature has clearly shown that the mechanisms underlying α-HPV– and β-HPV–associated tumorigenesis are markedly different (Cubie, 2013; Egawa et al., 2015; Venuti et al., 2019). Whereas α-HPVs are known to persist throughout neoplastic development, giving rise to tumors dependent on the E6 and E7 viral oncoproteins, β-HPVs are responsible for far more transient infections, mainly acting as cofactors of UV light at early stages of skin carcinogenesis (Akgül et al., 2006; Basukala and Banks, 2021; Gheit, 2019; Tommasino, 2017).

β-HPV–induced skin lesions primarily develop in immunocompromised subjects where the inability of the host to clear the infection favors high viral replication rates, leading to intraepidermal proliferative lesions often progressing to bona fide skin cancer (Howley and Pfister, 2015; Quint et al., 2015). These viruses were first discovered in patients suffering from epidermodysplasia verruciformis (EV), an autosomal recessive skin disease that specifically predisposes individuals to superinfection by β-HPV types (Béziat et al., 2021; Pfister, 2003). Indeed, high viral loads of HPV5 and HPV8 are found in the affected skin of patients with EV, where they can exert their full transforming potential, giving rise to multiple keratinocyte carcinomas (KCs), especially in sun-exposed areas (e.g., forehead) (Borgogna et al., 2012; Dell'Oste et al., 2009; Landini et al., 2012; Zavattaro et al., 2008). Importantly, nonsense sequence variation in two

[1]*Virology Unit, Department of Translational Medicine, Novara Medical School, Novara, Italy;* [2]*European Cancer Stem Cell Research Institute, School of Biosciences, Cardiff University, Cardiff, United Kingdom;* [3]*Virology Unit, Department of Public Health and Pediatric Sciences, Turin Medical School, Turin, Italy;* [4]*Center for Translational Research on Autoimmune and Allergic Disease (CAAD), Novara Medical School, Novara, Italy; and* [5]*Pathology Unit, Department of Health Sciences, Novara Medical School, Novara, Italy*

Correspondence: Marisa Gariglio, Department of Translational Medicine, University of Piemonte Orientale, Via Solaroli, Novara 17 - 28100, Italy. E-mail: marisa.gariglio@med.uniupo.it

Abbreviations: EV, epidermodysplasia verruciformis; HPV, human papillomavirus; KC, keratinocyte carcinoma; OTR, organ transplant recipient; PCNA, proliferating cell nuclear antigen

Received 26 December 2021; revised 9 October 2022; accepted 24 October 2022; accepted manuscript published online 5 December 2022; corrected proof published online 5 January 2023

adjacent genes, named *EVER1* and *EVER2*, have been associated with enhanced KC incidence in some consanguineous families and sporadic cases (Orth, 2006; Ramoz et al., 2002). The presence of a mutation in either of these two genes can in fact weaken EVER-mediated host restriction, thereby favoring β-HPV replication (Lazarczyk et al., 2009). In addition, patients with EV carrying homozygous null mutations in the *CIB1* gene encoding CIB1, another potential restriction factor against HPV, have also been reported (de Jong et al., 2018; Vahidnezhad et al., 2019). Intriguingly, EV-like phenotypes have also been consistently observed in patients with different immune defects—mostly T-cell immunodeficiency—that do not harbor any mutations in the *EVER* genes, indicating that dysregulated immunosurveillance may also facilitate β-HPV replication in the skin, thereby altering tissue homeostasis (Béziat et al., 2021; Borgogna et al., 2014a; Landini et al., 2014; Saluzzo et al., 2021; Uitto et al., 2022).

Another group of patients with an EV-like skin phenotype is represented by organ transplant recipients (OTRs), who display an overall risk of developing KC 100 times greater than the general population (Bouwes Bavinck et al., 2010). In these patients, the main risk factors of skin cancer development are (i) impaired immunosurveillance, due to the anti-rejection immunosuppressive regimen; (ii) UVR; and (iii) β-HPV infection (Hufbauer and Akgül, 2017; Rollison et al., 2019; Tampa et al., 2020; Tommasino, 2019; Venuti et al., 2019; Zhao et al., 2021). Fittingly, we have previously reported active β-HPV infection—as judged by HPV E4-positive immunostaining of OTR skin biopsies—in premalignant lesions, such as actinic keratoses, as well as in the hyperplastic edges of KCs. Of note, although the $E4^+$ areas were mainly found within the disorganized epithelium of actinic keratoses lesions, in more advanced KCs, they were always localized in the adjacent pathological epithelium. Furthermore, we detected MCM7 expression extending to the upper epithelial layers of $E4^+$ areas, indicating that the epithelial cells were actively proliferating in areas of productive viral infection (Borgogna et al., 2018, 2014b). In addition, a series of seroepidemiological studies have associated the presence of anti–β-HPV antibodies with skin cancer in OTRs, and PCR-based studies have identified β-HPV DNA in over 80% of skin tumors from these patients (Antonsson et al., 2013; Bouwes Bavinck et al., 2018, 2010; Genders et al., 2015; Proby et al., 2011; Rollison et al., 2021; Weissenborn et al., 2005). Although a large body of evidence has been gathered in humans, the impact of immunosuppression in a β-HPV mouse model is still unknown.

In this study, by crossing $Rag2^{-/-}$ mice—lacking both T and B cells (Hao and Rajewsky, 2001)—with K14-HPV8–transgenic mice, which harbor the entire early region of the HPV8 genotype driven by the K14 promoter, allowing skin-specific expression of the transgenes (Schaper et al., 2005), we have generated an immunodeficient mouse model named $Rag2^{-/-}$:K14-HPV8.

We show that the kinetics of papilloma development in $Rag2^{-/-}$:K14-HPV8 is significantly more accelerated than that of immunocompetent $Rag2^{+/+}$:K14-HPV8 mice, with lesions spreading to the entire skin very quickly after birth. We also report that $Rag2^{-/-}$:K14-HPV8 mice display persistence of UV-damaged cells in the epithelium, increased number of mast cells in the dermis, enhanced inflammatory cytokine release, and rapid papilloma development, suggesting that these *Rag2*-deficient HPV8-transgenic mice are much more sensitive to UVB-induced skin inflammation than their normo-competent HPV8 counterparts.

RESULTS AND DISCUSSION

To recapitulate the therapy-induced immunosuppressed setting of OTRs, who display defects in both arms of adaptive immunity (Ritter and Pirofski, 2009; Roberts and Fishman, 2021), and more generally of individuals with a compromised immune system, we generated HPV8-transgenic mice carrying *Rag2* mutations ($Rag2^{-/-}$:K14-HPV8), which lack B and T cells (Supplementary Figure S1). To rule out any bias related to the genetic background, mice were backcrossed to obtain a pure FVB/N background of the parental mouse line $Rag2^{+/+}$:K14-HPV8 in the immunodeficient genotype. Spontaneous papilloma development in $Rag2^{-/-}$:K14-HPV8 versus in $Rag2^{+/+}$:K14-HPV8 mice was assessed weekly by visual inspection of the skin for at least 25 weeks. Within 1 month after birth, $Rag2^{-/-}$:K14-HPV8 mice displayed smaller size, rough skin, and sparse hair development in comparison with $Rag2^{+/+}$:K14-HPV8 controls (Figure 1a and b). This unhealthy phenotype worsened over time, as shown in the representative images of $Rag2^{-/-}$:K14-HPV8 mice aged 5 months (Figure 1b, left-hand panel). In fact, these mice developed a severe skin phenotype characterized by dry, reddish, and scaly skin, exhibiting a series of papilloma-like proliferative lesions extending to all cutaneous skin causing alopecia. By contrast, the skin of $Rag2^{+/+}$:K14-HPV8 mice looked normal, with the sole exception of very few well-localized papilloma-like lesions usually restricted to the back (Figure 1b, right-hand panel). By the age of 25 weeks, all $Rag2^{-/-}$:K14-HPV8 mice had to be killed for ethical reasons. Notably, the lesions started to appear also on the legs at around age 12 weeks (see Supplementary Figure S2), a site that has never been reported to be affected in $Rag2^{+/+}$:K14-HPV8 genotype, even in very old mice (Schaper et al., 2005). As expected, $Rag2^{+/+}$ mice lived normally, and the lesions were limited to the dorsal skin. Strikingly, a large fraction of $Rag2^{-/-}$:K14-HPV8 mice developed papilloma at earlier time points than $Rag2^{+/+}$:K14-HPV8 mice (33% [n = 10] vs. 0% at age 10 weeks; $P < 0.05$) (Figure 1c). At age 24 weeks, 86% of the $Rag2^{-/-}$:K14-HPV8 mice (n = 26) had papilloma-like lesions, whereas they were visible only in 24% (n = 6) of $Rag2^{+/+}$:K14-HPV8 mice, indicating statistically significant differences between the two genotypes ($P < 0.0001$). All mice were observed and examined weekly, measuring the width and length of the lesions with a caliper along with their expansion in the whole skin from the abdomen and back. Individual percentages of affected skin areas were calculated as reported in Supplementary Figure S3.

The extension of the lesions—in terms of expansion of the affected skin area—was significantly greater in $Rag2^{-/-}$:K14-HPV8 than in $Rag2^{+/+}$:K14-HPV8 mice. As shown in Figure 1d, $Rag2^{-/-}$:K14-HPV8 mice that were old displayed skin lesions that spread diffusely to most of the skin surface, with the percentage of affected skin significantly higher in these mice than in their immunocompetent counterparts ($P < 0.0001$ at age

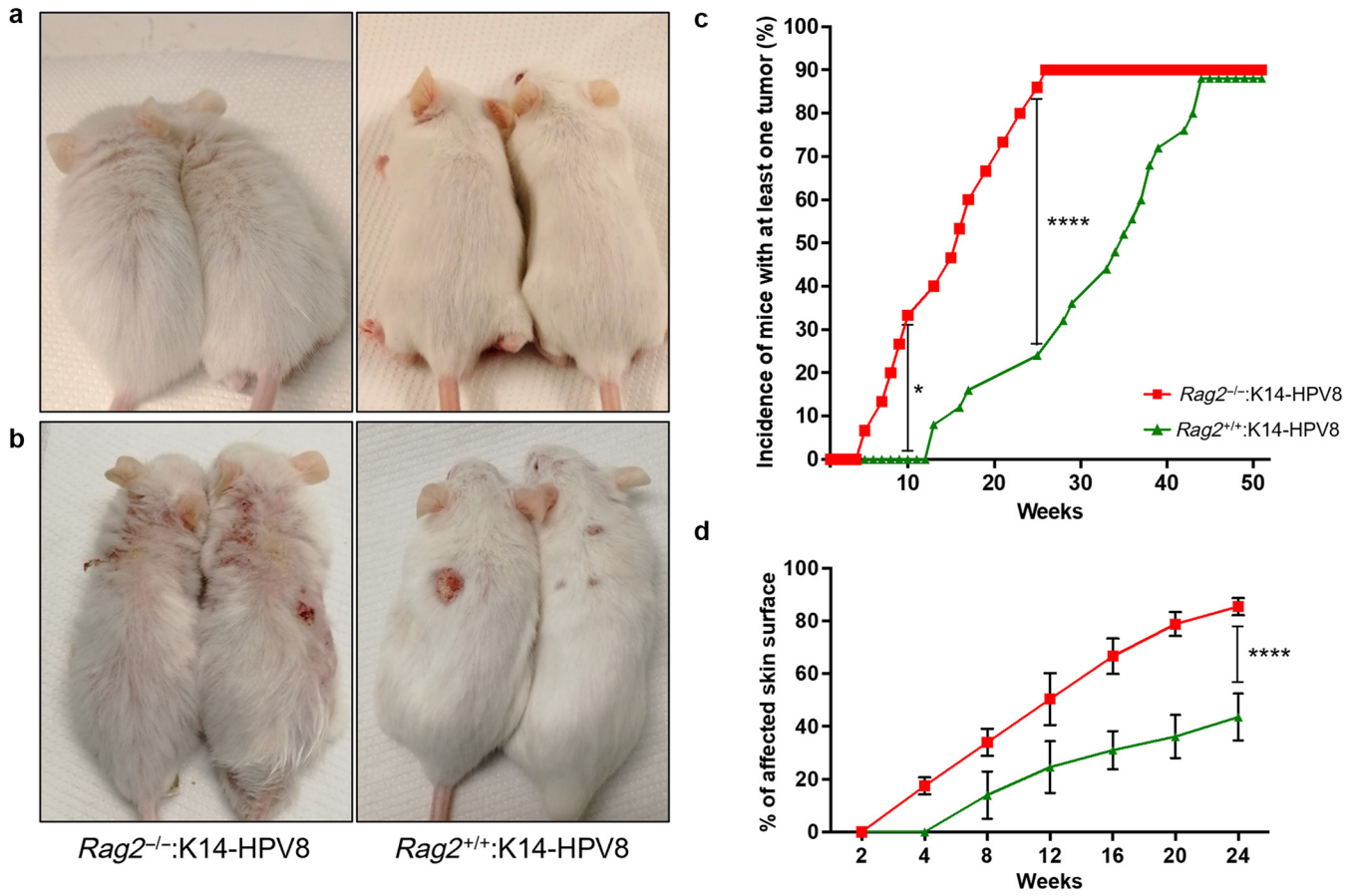

Figure 1. Enhanced tumor formation and expansion in *Rag2*$^{-/-}$:K14-HPV8 versus in *Rag2*$^{+/+}$:K14-HPV8 mice. Representative pictures of *Rag2*$^{-/-}$:K14-HPV8 (left) and *Rag2*$^{+/+}$:K14-HPV8 (right) mice at ages (**a**) 1 and (**b**) 5 months. (**c**) Tumor incidence and (**d**) percentage of affected skin in *Rag2*$^{-/-}$:K14-HPV8 (red line, n = 30) versus in *Rag2*$^{+/+}$:K14-HPV8 (green line, n = 25) as a function of time. *Rag2*$^{-/-}$:K14-HPV8 mice were observed until week 25 after birth and then killed for ethical reasons, whereas *Rag2*$^{+/+}$:K14-HPV8 mice were observed until age 50 weeks. In **c** and **d**, Fischer's exact test was performed at week 24. *$P < 0.05$ and ****$P < 0.0001$. In **c**, data are presented as mean ± SD. The formula to calculate the percentage of the affected skin is depicted in Supplementary Figure S3. HPV, human papillomavirus.

24 weeks). When killed, 2 of the 30 *Rag2*$^{-/-}$:K14-HPV8 mice analyzed showed lesions macroscopically characterized by the presence of necrotic areas and ulcerations, reminiscent of those tumors arising in *Rag2*$^{+/+}$:K14-HPV8, which were histologically described as squamous cell carcinoma (Supplementary Figure S4) (Schaper et al., 2005).

Histological analysis and measurement of the epidermal thickness of the skin obtained from healthy areas of the different genotypes—six mice aged 4 months for each genotype—did not reveal any significant difference in terms of epidermal thickness or proliferation in *Rag2*$^{-/-}$:K14-HPV8 versus in *Rag2*$^{+/+}$:K14-HPV8 mice (100 ± 16 vs. 77 ± 25 μm, respectively) (Figure 2a and b, left panel). The epidermis of both HPV8-transgenic genotypes was consistently thicker than that of their nontransgenic counterparts, that is, wild type and *Rag2*$^{-/-}$ mice (33 ± 5 and 37 ± 7 μm, respectively). Likewise, the proliferation rate, as determined by the number of proliferating cell nuclear antigen (PCNA)-positive cells, was significantly higher in the epidermis of transgenic mice than in that of nontransgenic ones, with higher significance in the *Rag2*$^{-/-}$ background (Rag2$^{+/+}$:K14-HPV8: 67 ± 9% vs. wild type: 40 ± 17% of PCNA-positive cells, $P < 0.05$; *Rag2*$^{-/-}$:K14-HPV8: 77 ± 12% vs. *Rag2*$^{-/-}$: 42±16% of PCNA-positive cells, $P < 0.01$), whereas no significant differences were found between *Rag2*$^{-/-}$:K14-HPV8 and *Rag2*$^{+/+}$:K14-HPV8 (Figure 2b, right panel).

Because we observed that the dermis of the two transgenic genotypes was massively populated by mast cells (Figure 2a) and given the controversy over the potential impact of these cells on HPV-driven carcinogenesis (Antsiferova et al., 2013; Biswas et al., 2014; Ghouse et al., 2018; Kaukinen et al., 2015; Rahkola et al., 2019; Siebenhaar et al., 2014), we sought to estimate the proportion of mast cells in our panel of mouse genotypes. Although the increased number of mast cells in *Rag2*$^{-/-}$:K14-HPV8 mice versus that of their normal counterparts was statistically significant (wild type: 101 ± 36 vs. *Rag2*$^{-/-}$:K14-HPV8: 232 ± 101 cells/mm^2, $P < 0.05$), no substantial difference in mast cell accumulation was observed in *Rag2*$^{-/-}$:K14-HPV8 versus in *Rag2*$^{+/+}$:K14-HPV8 mice (Figure 2b, middle panel).

Altogether these findings indicate that HPV8-driven skin tumorigenesis is significantly enhanced in a *Rag2*$^{-/-}$ versus in *Rag2*$^{+/+}$ background. Although the skin lesions appeared at early ages and expanded much faster in *Rag2*-null mice, no significant differences were observed with regard to the standard histological markers of proliferation analyzed. To

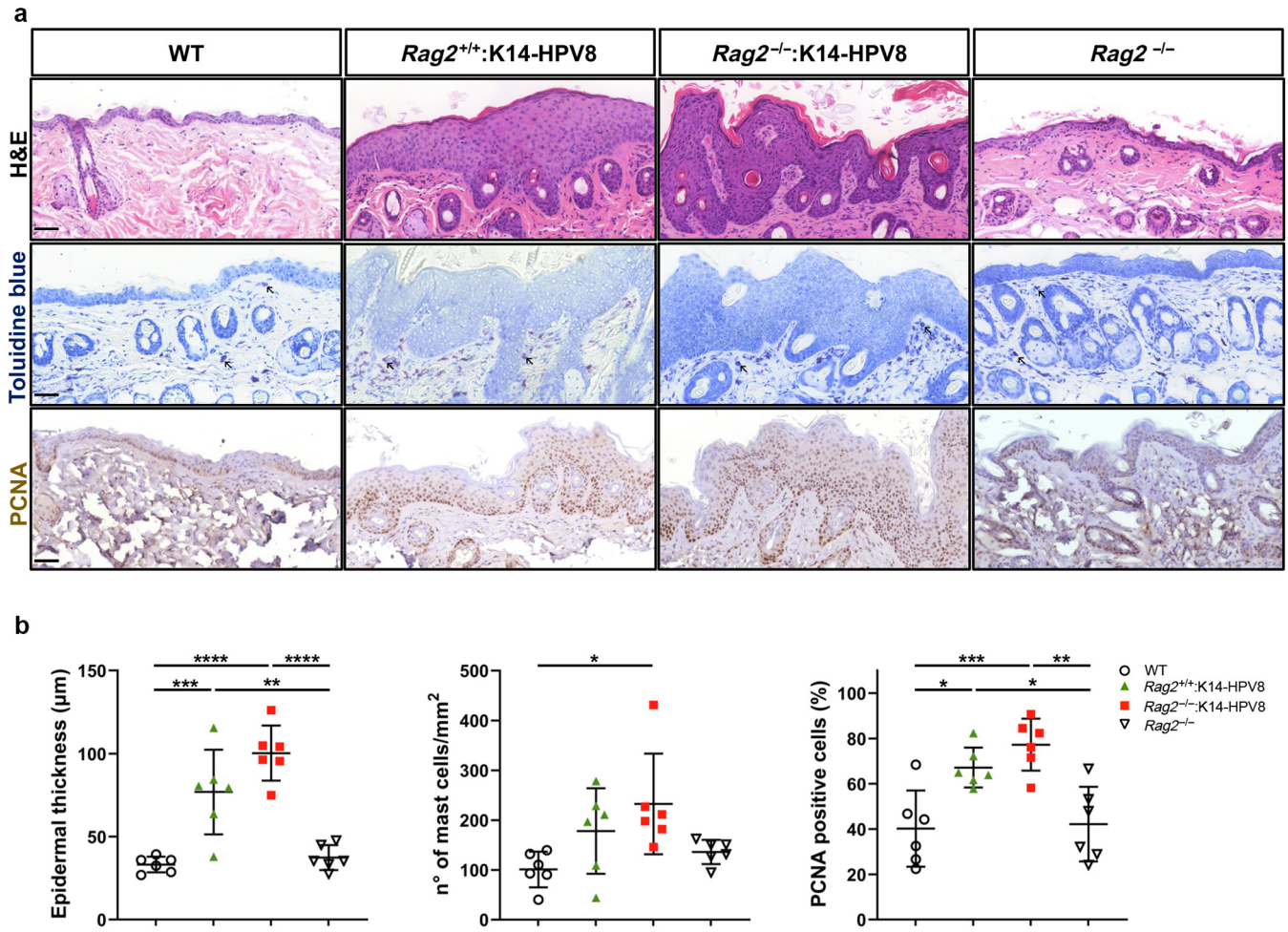

Figure 2. Histological and immunohistochemical characterization of the skin from *Rag2*$^{-/-}$:K14-HPV8 versus that from *Rag2*$^{+/+}$:K14-HPV8. (**a**) Representative images of H&E (upper row), toluidine blue staining (middle row), or PCNA (brown) immunostaining (lower row) in nonlesional skin biopsies obtained from the indicated mouse genotypes. Bars = 50 μm. Black arrows indicate toluidine blue–positive cells. (**b**) Quantification of epidermal thickness (μm) (left panel), quantitative evaluation of mast cell infiltration in the dermis (number of mast cells/mm^2) (middle panel), and percentage of PCNA-positive cells in the epidermis. The average percentage was calculated on the basis of the total number of cells and the number of positively stained cells (right panel). Each symbol represents the mean value obtained by evaluating 10 tissue section areas from a single mouse (n = 6 for each genotype). Data are presented as mean ± SD. Statistical analysis was performed by classical one-way ANOVA followed by Tukey's post hoc test. *$P < 0.05$, **$P < 0.01$, ***$P < 0.001$, and ****$P < 0.0001$. All groups were compared, but only those that reached statistical significance are shown. HPV, human papillomavirus; PCNA, proliferating cell nuclear antigen.

ascertain whether transgene expression levels in the two HPV8-transgenic mouse genotypes may affect skin tumorigenesis, we measured *HPV8 E6* and *E7* mRNA levels by RT-qPCR in epidermal lysates of lesional skin from *Rag2*$^{-/-}$:K14-HPV8 versus that from *Rag2*$^{+/+}$:K14-HPV8 mice. As shown in Supplementary Figure S5, *E6* and *E7* mRNA expression levels did not significantly differ between the two mouse strains. The mean ΔCt (±SD) was 2.54 ± 1.78 versus 2.64 ± 1.10 for *E6* transcripts and 3.69 ± 0.89 versus 2.54 ± 0.77 for *E7* transcripts in *Rag2*$^{-/-}$:K14-HPV8 and *Rag2*$^{+/+}$:K14-HPV8 mice, respectively.

Because the major risk factor contributing to skin cancer development is UVB exposure, either alone or in synergy with β-HPV infection, especially in immunosuppressed individuals, we next assessed the effects of a low dose of UVB exposure on the skin of *Rag2*$^{-/-}$:K14-HPV8 versus that of *Rag2*$^{+/+}$:K14-HPV8 mice. To this end, mice aged 1 month were exposed to a single UVB dose (0.36 J/cm^2) (Figure 3a, left panel) and then monitored for skin lesion development by visual inspection. Much to our surprise, all UVB-treated *Rag2*$^{-/-}$:K14-HPV8 mice (n = 6) showed very rapidly clear signs of enhanced skin inflammation, with epidermal thickness and ruffling, quickly expanding to the entire surface of the skin—about 90% of the surface was ultimately affected 30 days post-UVB exposure ($P < 0.01$) (Figure 3a, right panel). This rapid skin deterioration prompted us to kill the mice by the age of 2 months when papilloma-like lesions were macroscopically evident in many areas of the skin. As expected from the very low UVB dose used and the single exposure, neither *Rag2*$^{+/+}$:K14-HPV8 nor nontransgenic control mice displayed any skin alterations over the 1-month observational period (Figure 3b, first row) (Hufbauer et al., 2015). When we looked at the histology of the skin in the different genotypes, we found that the epidermis from UVB-treated *Rag2*$^{-/-}$:K14-HPV8 mice had become thicker, with clear signs of papillomatosis and acanthosis, in comparison

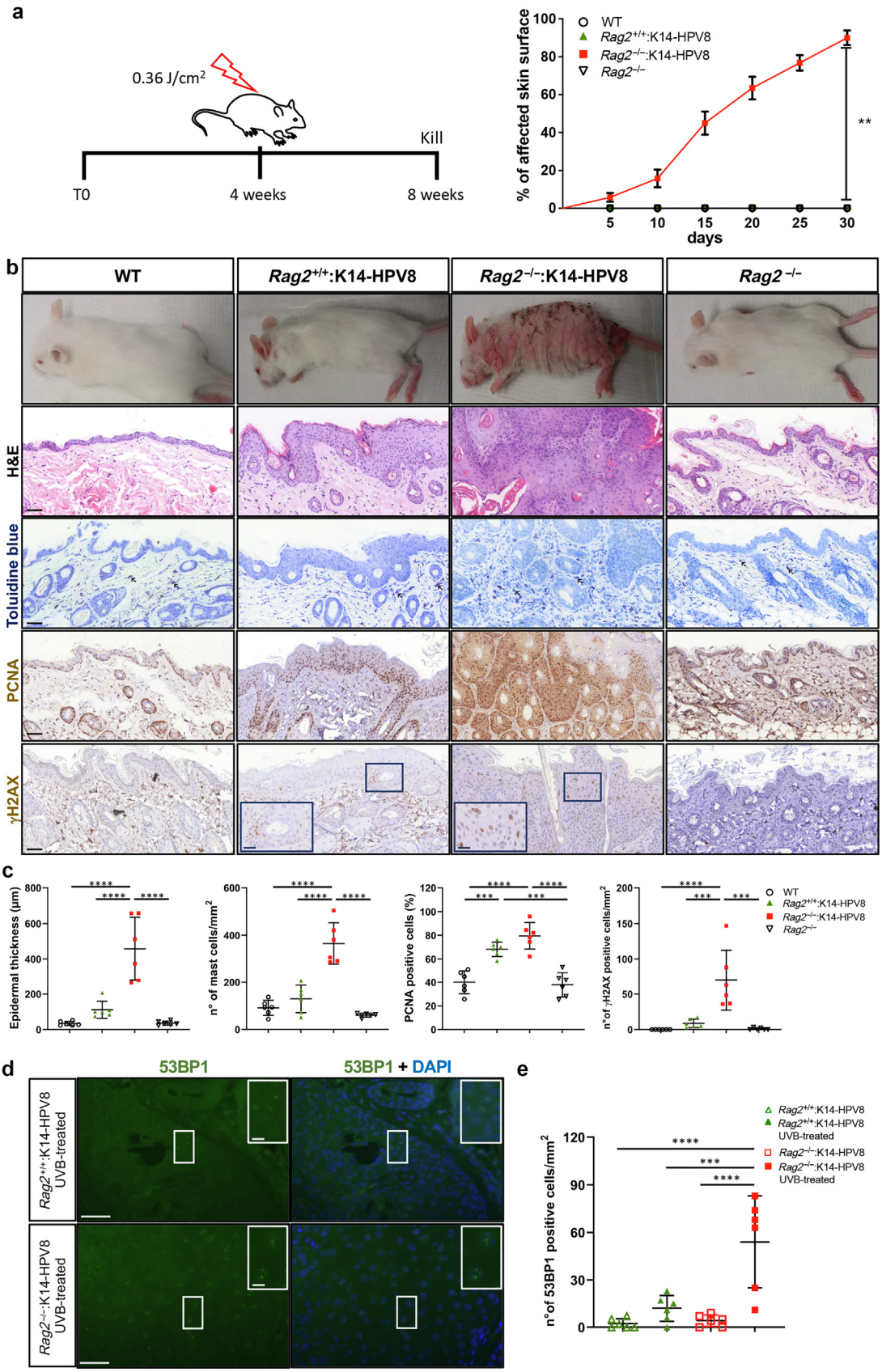

Figure 3. *Rag2*$^{-/-}$:K14-HPV8 mice are highly sensitive to UVB-induced inflammation and tumorigenesis. (**a**) Experimental timeline (left panel). Percentage of affected skin in WT, *Rag2*$^{+/+}$:K14-HPV8, *Rag2*$^{-/-}$:K14-HPV8, and *Rag2*$^{-/-}$ mice observed for 30 days after UVB irradiation (n = 6 for each genotype). The formula to calculate the percentage of the affected area is depicted in Supplementary Figure S3. Data are presented as mean ± SD. Fischer's exact test was performed on day 30 after UVB irradiation. $^{**}P < 0.01$ (right panel). (**b**) Phenotypic appearance of WT, *Rag2*$^{+/+}$:K14-HPV8, *Rag2*$^{-/-}$:K14-HPV8, and *Rag2*$^{-/-}$

with UVB-treated skin from *Rag2*$^{+/+}$:K14-HPV8 mice (457 ± 178 vs. 112 ± 48 μm, respectively, $P < 0.0001$) (Figure 3b and c). Consistent with the histology, the proliferation rate measured by PCNA staining in the skin from UVB-treated *Rag2*$^{-/-}$:K14-HPV8 mice was significantly higher than that from UVB-treated *Rag2*$^{+/+}$:K14-HPV8 mice (Figure 3b and c). Congruently, significant differences in epidermal thickness were also found in the skin from UVB-treated *Rag2*$^{-/-}$:K14-HPV8 versus that of untreated mice, whereas no differences were found in the skin from UVB-treated versus in that of untreated *Rag2*$^{+/+}$:K14-HPV8 mice (Supplementary Figure S6). Notably, the number of mast cells present in the dermis of UVB-treated *Rag2*$^{-/-}$:K14-HPV8 was also significantly greater than that observed in similarly treated dermis of *Rag2*$^{+/+}$:K14-HPV8 mice (365 ± 87 vs. 129 ± 58 cells/mm^2 respectively, $P < 0.001$) (Figure 3b and c).

The E6 and E7 oncoproteins have been reported to interfere with DNA damage repair, thus leading to the accumulation of DNA photoproducts, such as cyclobutane pyrimidine dimers, which in turn contribute to genomic instability and cancer progression in many experimental models of HPV-induced skin carcinogenesis (Deshmukh et al., 2016; Hasche et al., 2017; Hufbauer et al., 2015; Hufbauer and Akgül, 2017). Thus, we decided to assess the extent of phosphorylated H2AX (γH2AX) nuclear staining, a surrogate marker of DNA damage and chromosomal instability, in mice killed 1 month after UVB exposure. As expected from the very long time passed from the exposure to such a low UVB dose, UVB-exposed *Rag2*$^{+/+}$:K14-HPV8 mice showed very few γH2AX-positive nuclei in the skin (9 ± 6 cells/mm^2), whereas none were detected in their parental counterparts. Surprisingly, a significantly increased number of γH2AX-positive nuclei were found in the skin from UVB-treated *Rag2*$^{-/-}$:K14-HPV8 mice (70 ± 42 cells/mm^2) (Figure 3b and c). To strengthen these data, we stained serial skin sections with an antibody recognizing 53BP1, another marker of damaged DNA recruited to double-strand breaks (Chang et al., 2017; Lei et al., 2022; Rappold et al., 2001). Consistent with our previous γH2AX staining, we observed an increased number of cells displaying 53BP1-positive foci (Figure 3d and e) in the skin from UVB-treated *Rag2*$^{-/-}$:K14-HPV8 versus from similarly treated *Rag2*$^{+/+}$:K14-HPV8 mice (56 ± 39 cells/mm^2 and 8 ± 9 cells/mm^2, respectively, $P < 0.001$). Notably, the number of cells with 53BP1 foci dropped dramatically in the skin from untreated *Rag2*$^{-/-}$:K14-HPV8 mice when compared with that of their UVB-treated counterparts (56 ± 39 cells/mm^2 vs. 4 ± 4 cells/mm^2, respectively, $P < 0.0001$).

To assess whether differential cytokine expression in the skin could account for the aberrant reaction to UVB observed in *Rag2*$^{-/-}$:K14-HPV8 mice, skin protein extracts were analyzed by BioPlex arrays. As shown in Figure 4 and Supplementary Figure S7, the expression levels of several inflammatory cytokines/chemokines (e.g., G-CSF, CXCL-1, IL-6, monocyte chemotactic protein-1, and IL-1β) were significantly upregulated in the inflamed skin areas of UVB-exposed *Rag2*$^{-/-}$:K14-HPV8 mice in comparison with those measured in noninflamed and non-UVB–exposed skin areas from the same mice. In line with the lack of inflammation observed in *Rag2*$^{+/+}$:K14-HPV8 and parental mice on UVB exposure, none of the cytokines/chemokines mentioned earlier was upregulated in these genotypes.

The current concepts of enhanced skin cancer development in patients with immune defects (e.g., OTRs) emphasize the important role of impaired immunosurveillance combined with enhanced susceptibility to UVB-induced DNA damage in this setting (Rollison et al., 2019; Tommasino, 2017). In addition to these two fundamental risk factors, a series of molecular and epidemiological data support a functional contribution of some cutaneous β-HPV genotypes, especially HPV8 and HPV5, in potentiating UVB-mediated destabilization of the genome and preventing cell cycle arrest that would normally trigger DNA repair mechanisms (Dacus and Wallace, 2021; Giampieri and Storey, 2004; Wallace et al., 2015). In particular, β-HPV oncoproteins have been shown to disrupt the cellular response to UV exposure by dampening DNA repair mechanisms. The interaction of E6 with the pro-apoptotic protein BAK prevents its accumulation after UV-irradiation–induced DNA damage, thus reducing apoptosis of damaged cells (Holloway et al., 2015; Simmonds and Storey, 2008; Underbrink et al., 2008). Upstream of the inhibition of apoptosis, β-HPV E6 expression deregulates the G1 to S-phase cell cycle checkpoint in response to DNA damage, which in turn allows cells with persistent DNA damage to proliferate (Giampieri and Storey, 2004; Wendel and Wallace, 2017). These effects arise from the interaction of β-HPV E6 with acetyltransferase p300, an important coactivator of DNA damage repair gene transcription (Dacus and Wallace, 2021; Marthaler et al., 2017; Smola, 2017; Wallace and Galloway, 2014). The reduced availability of the DNA damage repair kinases ataxia telangiectasia mutated and ataxia telangiectasia mutated and Rad3-related as well as BRCA1 and BRCA2 in β-HPV E6–expressing cells in vitro significantly delays the repair of

mice 30 days after UVB irradiation (first row). Representative images of H&E (second row), toluidine blue (third row), PCNA, and γH2AX (brown with nuclear counterstaining in blue; fourth and fifth row, respectively) immunohistochemical staining of UVB-irradiated skin from the indicated mouse genotype are shown. Bars = 50 μm. Black arrows indicate toluidine blue–positive cells. The region shown in the inset corresponds to the square highlighted in the γH2AX images. Bars (inset) = 20 μm. (**c**) The first panel from the left indicates the quantification of epidermal thickness (μm), the second panel indicates the quantitative evaluation of mast cell infiltration in the dermis (number of mast cells/mm^2), the third panel indicates the percentage of PCNA-positive cells in the epidermis (the mean percentage was calculated on the basis of the total number of cells and the number of positively stained cells), the fourth panel indicates the quantification of γH2AX-positive cells in the epidermis (number of γH2AX-positive cells /mm^2). Each symbol represents the mean value obtained by evaluating 10 tissue section areas from an individual mouse (n = 6 for each genotype). Data are presented as mean ± SD. Statistical analysis was performed by classical one-way ANOVA followed by Tukey's post hoc test. ***$P < 0.001$ and ****$P < 0.0001$. All groups were compared, but only those that reached statistical significance are shown. (**d**) Representative images of 53BP1 immunofluorescent staining of UVB-irradiated skin from the indicated mouse genotypes. Bars = 50 μm. The region shown in the inset corresponds to the square highlighted in the 53BP1 images. Bars (inset) = 5 μm. (**e**) Quantification of 53BP1-positive cells in the epidermis (number of 53BP1-positive cells/mm^2) from UVB-treated *Rag2*$^{+/+}$:K14-HPV8 or *Rag2*$^{-/-}$:K14-HPV8 mice. Each symbol represents the mean value obtained by evaluating 10 tissue section areas from an individual animal (n = 6 for each genotype). Data are presented as mean ± SD. Statistical analysis was performed by classical one-way ANOVA followed by Tukey's post hoc test. ***$P < 0.001$ and ****$P < 0.0001$. All groups were compared, but only those that reached statistical significance are shown. HPV, human papillomavirus; PCNA, proliferating cell nuclear antigen; WT, wild type.

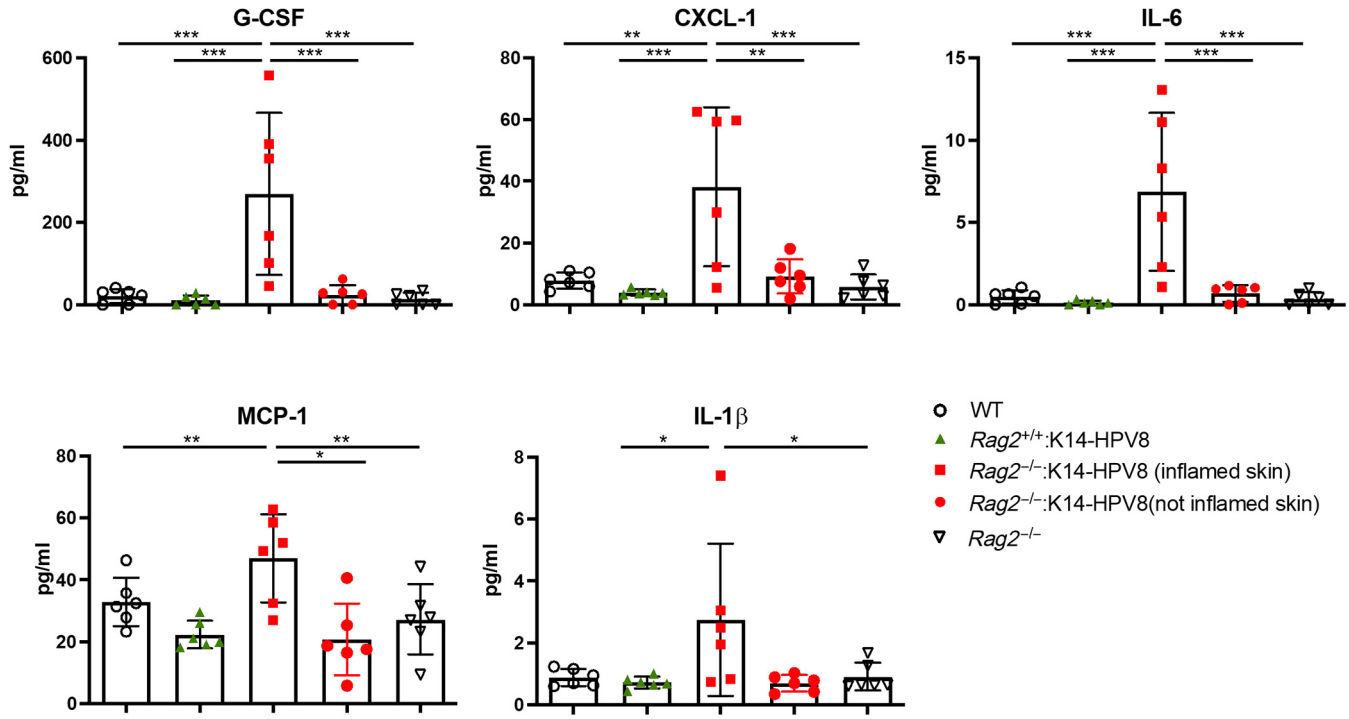

Figure 4. Enhanced cytokine/chemokine induction in *Rag2*$^{-/-}$:K14-HPV8 mice on UVB exposure. Quantification of G-CSF, CXCL-1, IL-6, MCP-1, and IL-1β cytokines in UVB-irradiated skin homogenates from WT, *Rag2*$^{+/+}$:K14-HPV8, *Rag2*$^{-/-}$:K14-HPV8 (inflamed or non-inflamed skin), and *Rag2*$^{-/-}$ mice by Bio-Plex Pro Mouse Cytokine 23-Plex Immunoassay. Each symbol represents the value of an individual mouse (n = 6 for each genotype). Data are represented as mean ± SD. Statistical analysis was performed by classical one-way ANOVA followed by Tukey's post hoc test. *$P < 0.05$, **$P < 0.01$, and ***$P < 0.001$. HPV, human papillomavirus; MCP-1, monocyte chemotactic protein-1; WT, wild type.

UV-induced cyclobutane pyrimidine dimer while increasing the UV-induced frequency of DNA double-stranded breaks (Wallace et al., 2015, 2012). In these cells, delayed γH2AX foci resolution—a known marker of DNA double-stranded breaks—after exposure to ionizing radiation has been reported (Wallace et al., 2015). Because skin cancer in humans arises from a long-lasting multistep process where β-HPV infection is mostly active in the early stages of the disease and usually not maintained in the overt cancer, it has always been challenging to definitely prove β-HPV contribution to tumorigenesis in vivo.

In this study, using an immunocompromised skin-specific HPV8-transgenic mouse model, we provide the proof of concept that lack of immunosurveillance and persistence of UV-damaged cells are both contributing to enhanced skin cancer development and inflammation in KCs overexpressing HPV8 E6 and E7 oncoproteins. Specifically, we show that the lack of immunosurveillance is critical for tumor formation in terms of both early development and expansion. In the first weeks after birth, when the skin of *Rag2*$^{+/+}$:K14-HPV8 mice looks fully normal, the skin of their *Rag2*-deficient counterparts is already characterized by an unhealthy inflamed phenotype, which is quickly populated by multiple and confluent papilloma-like lesions covering the entire skin surface. This enhanced tumor formation does not appear to be associated with any changes in skin histology in immunocompromised versus in immunocompetent transgenic mice, including the abnormal expansion of LRIG1^{+} KC stem cells in the upper hair follicles, a phenomenon occurring in both genotypes (Lanfredini et al., 2017).

Another important finding from our in vivo model is the demonstration that the KCs expressing HPV8 early proteins display reduced ability to clear UVB-damaged cells, as indicated by the persistence of a remarkable number of γH2AX and 53BP1 foci after 1 month from exposure to a single low dose of UVB. In addition, this accumulation of damaged cells is accompanied by an increased skin-specific expression of a series of inflammatory cytokines/chemokines and enhanced recruitment of mast cells. Altogether, these findings perfectly fit with the skin inflammatory phenotype observed in *Rag2*$^{-/-}$:K14-HPV8 mice, along with the enhanced and prolonged reaction to UVB exposure. In addition, the cytokines/chemokines found upregulated in our setting are known to be crucial in skin inflammation and enhanced cancer development in a panel of experimental models (Fitsiou et al., 2021; Mantovani et al., 2008; Neagu et al., 2019). Although several studies have already shown a cause–effect relationship among HPV infection, UVB exposure, and skin cancer development in transgenic mice expressing HPV20, HPV38, or HPV8, the impact of immunosuppression on tumorigenesis had not been investigated in these animal models (Deshmukh et al., 2016; Michel et al., 2006; Viarisio et al., 2018, 2011).

Although this study does not provide mechanistic details about the molecular pathways driving skin inflammation and cancer, for which further studies are clearly needed, our mouse model shows that the coexistence of immune defects, β-HPV infection, and UVB exposure promotes the formation of a highly inflammatory environment in the skin, partly explained by the persistence of UVB-damaged cells,

enhanced release of inflammatory cytokines/chemokines, and abnormal expansion/recruitment of professional inflammatory cells (e.g., mast cells).

Overall, this mouse model very much resembles the phenotype of OTRs who usually developed inflamed skin, especially in sun-exposed areas, a process also known as field cancerization (Braakhuis et al., 2003; Gilchrest, 2021; Olivero et al., 2018; Vanharanta and Massagué, 2012; Willenbrink et al., 2020). Finally, very likely owing to the different experimental model used, our manuscript hardly fit with the data reported by Strickley et al. (2019), which argue that infection of the skin with commensal cutaneous papillomaviruses induces T-cell immunity and inhibits skin carcinogenesis in immunocompetent mice.

MATERIALS AND METHODS

Generation of *Rag2*$^{-/-}$:K14-HPV8−transgenic mice, genotyping, and treatments

The K14-HPV8−transgenic mice (Schaper et al., 2005) were kindly provided by the group of Herbert Pfister and Baki Akgül, University of Cologne (Cologne, Germany). The *Rag2*$^{-/-}$ mice (Hao and Rajewsky, 2001) were kindly provided by Cecilia Garlanda from the Humanitas Research Center (Milan, Italy). Briefly, *Rag2*$^{-/-}$ mice were crossed with K14-HPV8 mice to produce the first filial generation (F1) with mixed genetic backgrounds (FVB/N and C57BL/6). The *Rag2*$^{+/-}$ progeny was backcrossed with K14-HPV8 mice to obtain the first backcross generation (N1). The *Rag2*$^{+/-}$ mice from the N1 generation were backcrossed with K14-HPV8 mice for 10 generations to yield the N10 generation with pure FVB/N background. The N10 mice with *Rag2*$^{+/-}$:K14-HPV8 or *Rag2*$^{+/-}$ genotypes were intercrossed to obtain the genotype *Rag2*$^{-/-}$:K14-HPV8 (Supplementary Figure S1). Mice were housed under pathogen-free conditions in our animal facilities in accordance with "The Guide for the Care and Use of Laboratory Animals," and the experimentation was approved by the Italian Ministry of Health (agreement number 500/2019-PR).

Genomic DNA was isolated from tail biopsies of mice aged 10 days by the phenol-chloroform standard method. PCR analysis to detect the presence of the *Rag2* gene was performed using a set of three primers designed to amplify the DNA sequence of Rag 2 exon 3 and the replacement gene (forward primer: 5′−CAAGGA CGCTCTAGGAATGCA-3′, reverse primers: wtREV 5′-GCTATGT-TATGACCCACTGTTAC-3′, and mutREV 5′-GCTTTACGGTATCGCC GCTC-3′). PCRs were performed on a C1000 Touch thermal cycler (Bio-Rad Laboratories, Hercules, CA) using the following protocol: 95 °C for 3 minutes, 35 cycles of 94 °C for 30 seconds; 55 °C for 30 seconds; 72 °C for 20 seconds; and a final extension period at 72 °C for 5 minutes. PCR products were separated by 1.5% agarose−TAE gel electrophoresis, and SYBR safe DNA gel stain (Invitrogen, Waltham, MA) was used to detect the separated bands. RAG2 band sizes were expected to be 324 base pair for the wild type allele and 419 base pair for the mutant allele. The PCR protocols used for the HPV8 transgenes have been described elsewhere (Schaper et al., 2005).

Calculation of the percentage of affected skin

All mice were weekly evaluated by measuring the width (w) and length (l) of the lesions and the whole skin from the abdomen and back with a caliper. Areas were calculated with the formula (A) = w × l. Each mouse's total lesional area was obtained through the sum of all the single lesion areas (A_1, A_2…), whereas the total skin area (A tot) was calculated by the sum of the abdominal and back areas. The percentage of affected skin areas was calculated as (lesional area/total skin area) × 100 as reported in Supplementary Figure S3.

RT-qPCR

The skin was incubated overnight with dispase II 0.5% (Sigma-Aldrich, St. Louis, MO) at 4 °C, and then the epidermis was mechanically separated from the dermis. Epidermal RNA was extracted using TRIzol (Thermo Fisher Scientific, Waltham, MA) and retrotranscribed using iScript cDNA synthesis kit (Bio-Rad Laboratories), and RT-qPCR analysis was performed as described (De Andrea et al., 2010; Lanfredini et al., 2017).

UVB irradiation

UVB radiation was generated by a UV device (9021, DELTA OHM, Caselle, Italy) equipped with a radiometric probe suitable for measuring radiation in the UV region B (UVB spectral range = 280−315 nm). Before UVB exposure, mice were anesthetized (2% isoflurane), and their back (4 cm^2) was shaved with an electric razor. Anesthetized mice were irradiated once with 0.36 J/cm^2 UVB at the shaved back (Marcuzzi et al., 2009). Mice were checked for 30 days twice a week for the appearance of tumors.

Histological and immunohistochemical analysis of the skin

Consecutive 5-μm thick tissue sections were cut from formalin-fixed, paraffin-embedded blocks; dewaxed; and rehydrated using standard procedures. Serial sections were stained with H&E, toluidine blue, or primary antibodies against PCNA (P8825 clone PC10, Sigma-Aldrich), γH2AX (clone JBW301, MilliporeSigma, Burlington, MA), and 53BP1 (clone E-10, Santa Cruz Biotechnology, Dallas, TX). Antigen unmasking was performed by microwaving the sections for 10 minutes in 10 mM citrate buffer at pH 6.0 (Vector Laboratories, Burlingame, CA). Slides were incubated overnight at 4 °C with primary antibodies diluted in 5% normal goat serum, stained by indirect immunoperoxidase with the substrate 3,3′-diaminobenzidine, counterstained with Mayer's hematoxylin, and mounted on slides using VectaMount mounting medium (Vector Laboratories). The epidermal thickness and the cell number for the quantification of mast cells, PCNA, γH2AX, and 53BP1-positive cells were recorded using Fiji software technology.

Cytokine BioPlex assay

Skin lysates were obtained from thawed, homogenized, and sonicated tissues using the BioPlex cell lysis kit (Bio-Rad Laboratories). Proteins were quantified using a BCA assay (Thermo Fisher Scientific). Tissue lysates were brought to 1 mg/ml using 1× PBS with 0.5% BSA, and 50 μl were added to each well. Cytokines were measured by BioPlex Pro mouse Cytokine 23-Plex Assay (Bio-Rad Laboratories) according to the manufacturer's instructions. Data were acquired and analyzed with a Luminex device using the Bio-Rad Bio-Plex System and Bio-Plex Manager Software.

Statistical analysis

All statistical analyses were performed using GraphPad Prism (GraphPad Software, San Diego, CA), version 6.00, for Windows; data are expressed as mean ± SD. For comparisons among three groups, means were compared using one-way ANOVA followed by Tukey's post hoc test. Fisher's exact test was used for the analysis of tumor incidence and lesional skin expansion. Significance was set at $P < 0.05$.

Data availability statement

Data supporting the findings of this study are available from the corresponding author on request. No datasets were generated during this study.

ORCIDs

Cinzia Borgogna: http://orcid.org/0000-0001-9973-2620
Licia Martuscelli: http://orcid.org/0000-0001-8320-7151
Carlotta Olivero: http://orcid.org/0000-0002-8961-6703
Irene Lo Cigno: http://orcid.org/0000-0001-5521-3642
Marco De Andrea: http://orcid.org/0000-0002-3188-5783
Valeria Caneparo: http://orcid.org/0000-0002-8210-3235
Renzo Boldorini: http://orcid.org/0000-0003-1183-2737
Girish Patel: http://orcid.org/0000-0003-1093-2875
Marisa Gariglio: http://orcid.org/0000-0002-5187-0140

CONFLICT OF INTEREST

The authors state no conflict of interest.

ACKNOWLEDGMENTS

This research was funded by the Italian Ministry for University and Research—MIUR (PRIN 2017) to CB, H2020-MSCA-IF-2017- 799829—SKin SCiENCE to CO, the AGING Project—Department of Excellence—DIMET, Università del Piemonte Orientale, and the Associazione Italiana per la Ricerca sul Cancro (IG2016) to MG. We are grateful to Herbert Pfister and Baki Akgül from the University of Cologne (Cologne, Germany) and Cecilia Garlanda from the Humanitas Research Center (Milan, Italy) for providing the K14-HPV8–transgenic mice and the *Rag2*$^{-/-}$ mice, respectively. We thank Marcello Arsura for critically reviewing the manuscript. The Bio-plex analyses were performed through the dedicated facilities at the Center for Translational Research on Autoimmune and Allergic Disease (Novara, Italy).

AUTHOR CONTRIBUTIONS

Conceptualization: MG, GP; Formal Analysis: CB, LM; Investigation: CB, LM, CO, VC, ILC; Methodology: MDA, CB, LM, CO, VC, ILC; Resources: MG, CB, CO; Supervision: MG; Visualization: CB, LM; Writing - Original Draft Preparation: MG, CB; Writing - Review and Editing: GP, MDA, LM, CO, RB

SUPPLEMENTARY MATERIAL

Supplementary material is linked to the online version of the paper at www.jidonline.org, and at https://doi.org/10.1016/j.jid.2022.10.023.

REFERENCES

Akgül B, Cooke JC, Storey A. HPV-associated skin disease. J Pathol 2006;208:165–75.

Antonsson A, Waterboer T, Bouwes Bavinck JN, Abeni D, de Koning M, Euvrard S, et al. Longitudinal study of seroprevalence and serostability of 34 human papillomavirus types in European organ transplant recipients. Virology 2013;436:91–9.

Antsiferova M, Martin C, Huber M, Feyerabend TB, Förster A, Hartmann K, et al. Mast cells are dispensable for normal and activin-promoted wound healing and skin carcinogenesis. J Immunol 2013;191:6147–55.

Basukala O, Banks L. The not-so-good, the bad and the ugly: HPV E5, E6 and E7 oncoproteins in the orchestration of carcinogenesis. Viruses 2021;13:1892.

Béziat V, Casanova JL, Jouanguy E. Human genetic and immunological dissection of papillomavirus-driven diseases: new insights into their pathogenesis. Curr Opin Virol 2021;51:9–15.

Biswas A, Richards JE, Massaro J, Mahalingam M. Mast cells in cutaneous tumors: innocent bystander or maestro conductor? Int J Dermatol 2014;53:806–11.

Borgogna C, Landini MM, Lanfredini S, Doorbar J, Bouwes Bavinck JN, Quint KD, et al. Characterization of skin lesions induced by skin-tropic α- and β-papillomaviruses in a patient with epidermodysplasia verruciformis. Br J Dermatol 2014a;171:1550–4.

Borgogna C, Lanfredini S, Peretti A, De Andrea M, Zavattaro E, Colombo E, et al. Improved detection reveals active β-papillomavirus infection in skin lesions from kidney transplant recipients [published correction appears in Mod Pathol 2014b;27:917] Mod Pathol 2014b;27:1101–15.

Borgogna C, Olivero C, Lanfredini S, Calati F, De Andrea M, Zavattaro E, et al. β-HPV infection correlates with early stages of carcinogenesis in skin tumors and patient-derived xenografts from a kidney transplant recipient cohort. Front Microbiol 2018;9:117.

Borgogna C, Zavattaro E, De Andrea M, Griffin HM, Dell'Oste V, Azzimonti B, et al. Characterization of beta papillomavirus E4 expression in tumours from epidermodysplasia verruciformis patients and in experimental models. Virology 2012;423:195–204.

Bouwes Bavinck JN, Feltkamp MCW, Green AC, Fiocco M, Euvrard S, Harwood CA, et al. Human papillomavirus and posttransplantation cutaneous squamous cell carcinoma: a multicenter, prospective cohort study. Am J Transplant 2018;18:1220–30.

Bouwes Bavinck JNB, Neale RE, Abeni D, Euvrard S, Green AC, Harwood CA, et al. Multicenter study of the association between Betapapillomavirus infection and cutaneous squamous cell carcinoma. Cancer Res 2010;70:9777–86.

Braakhuis BJM, Tabor MP, Kummer JA, Leemans CR, Brakenhoff RH. A genetic explanation of Slaughter's concept of field cancerization: evidence and clinical implications. Cancer Res 2003;63:1727–30.

Chang HHY, Pannunzio NR, Adachi N, Lieber MR. Non-homologous DNA end joining and alternative pathways to double-strand break repair. Nat Rev Mol Cell Biol 2017;18:495–506.

Cubie HA. Diseases associated with human papillomavirus infection. Virology 2013;445:21–34.

Dacus D, Wallace NA. Beta-genus human papillomavirus 8 E6 destabilizes the host genome by promoting p300 degradation. Viruses 2021;13:1662.

De Andrea M, Rittà M, Landini MM, Borgogna C, Mondini M, Kern F, et al. Keratinocyte-specific stat3 heterozygosity impairs development of skin tumors in human papillomavirus 8 transgenic mice. Cancer Res 2010;70:7938–48.

de Jong SJ, Créquer A, Matos I, Hum D, Gunasekharan V, Lorenzo L, et al. The human CIB1-EVER1-EVER2 complex governs keratinocyte-intrinsic immunity to β-papillomaviruses. J Exp Med 2018;215:2289–310.

Dell'Oste V, Azzimonti B, De Andrea M, Mondini M, Zavattaro E, Leigheb G, et al. High β-HPV DNA loads and strong seroreactivity are present in epidermodysplasia verruciformis. J Invest Dermatol 2009;129:1026–34.

Deshmukh J, Pofahl R, Pfister H, Haase I. Deletion of epidermal Rac1 inhibits HPV-8 induced skin papilloma formation and facilitates HPV-8- and UV-light induced skin carcinogenesis. Oncotarget 2016;7:57841–50.

Egawa N, Egawa K, Griffin H, Doorbar J. Human papillomaviruses; epithelial tropisms, and the development of neoplasia. Viruses 2015;7:3863–90.

Fitsiou E, Pulido T, Campisi J, Alimirah F, Demaria M. Cellular senescence and the senescence-associated secretory phenotype as drivers of skin photoaging. J Invest Dermatol 2021;141:1119–26.

Galloway DA, Laimins LA. Human papillomaviruses: shared and distinct pathways for pathogenesis. Curr Opin Virol 2015;14:87–92.

Genders RE, Mazlom H, Michel A, Plasmeijer EI, Quint KD, Pawlita M, et al. The presence of Betapapillomavirus antibodies around transplantation predicts the development of keratinocyte carcinoma in organ transplant recipients: a cohort study. J Invest Dermatol 2015;135:1275–82.

Gheit T. Mucosal and cutaneous human papillomavirus infections and cancer biology. Front Oncol 2019;9:355.

Ghouse SM, Polikarpova A, Muhandes L, Dudeck J, Tantcheva-Poór I, Hartmann K, et al. Although abundant in tumor tissue, mast cells have no effect on immunological micro-milieu or growth of HPV-induced or transplanted tumors. Cell Rep 2018;22:27–35.

Giampieri S, Storey A. Repair of UV-induced thymine dimers is compromised in cells expressing the E6 protein from human papillomaviruses types 5 and 18. Br J Cancer 2004;90:2203–9.

Gilchrest BA. Actinic keratoses: reconciling the biology of field cancerization with treatment paradigms. J Invest Dermatol 2021;141:727–31.

Hao Z, Rajewsky K. Homeostasis of peripheral B cells in the absence of B cell influx from the bone marrow. J Exp Med 2001;194:1151–64.

Hasche D, Stephan S, Braspenning-Wesch I, Mikulec J, Niebler M, Gröne HJ, et al. The interplay of UV and cutaneous papillomavirus infection in skin cancer development. PLoS Pathog 2017;13:e1006723.

Holloway A, Simmonds M, Azad A, Fox JL, Storey A. Resistance to UV-induced apoptosis by β-HPV5 E6 involves targeting of activated BAK for proteolysis by recruitment of the HERC1 ubiquitin ligase. Int J Cancer 2015;136:2831–43.

Howley PM, Pfister HJ. Beta genus papillomaviruses and skin cancer. Virology 2015;479–480:290–6.

Hufbauer M, Akgül B. Molecular mechanisms of human papillomavirus induced skin carcinogenesis. Viruses 2017;9:187.

Hufbauer M, Cooke J, van der Horst GTJ, Pfister H, Storey A, Akgül B. Human papillomavirus mediated inhibition of DNA damage sensing and repair drives skin carcinogenesis. Mol Cancer 2015;14:183.

Kaukinen A, Pelkonen J, Harvima IT. Mast cells express CYP27A1 and CYP27B1 in epithelial skin cancers and psoriasis. Eur J Dermatol 2015;25:548–55.

Kranjec C, Doorbar J. Human papillomavirus infection and induction of neoplasia: a matter of fitness. Curr Opin Virol 2016;20:129–36.

Kreuter A, Gambichler T, Pfister H, Wieland U. Diversity of human papillomavirus types in periungual squamous cell carcinoma. Br J Dermatol 2009;161:1262–9.

Lambert PF, Münger K, Rösl F, Hasche D, Tommasino M. Beta human papillomaviruses and skin cancer. Nature 2020;588:E20–1.

Landini MM, Borgogna C, Peretti A, Colombo E, Zavattaro E, Boldorini R, et al. α- and β-Papillomavirus infection in a young patient with an unclassified primary T-cell immunodeficiency and multiple mucosal and cutaneous lesions. J Am Acad Dermatol 2014;71:108–15.e1.

Landini MM, Zavattaro E, Borgogna C, Azzimonti B, De Andrea M, Colombo E, et al. Lack of EVER2 protein in two epidermodysplasia verruciformis patients with skin cancer presenting previously unreported homozygous genetic deletions in the EVER2 gene. J Invest Dermatol 2012;132:1305–8.

Lanfredini S, Olivero C, Borgogna C, Calati F, Powell K, Davies KJ, et al. HPV8 field cancerization in a transgenic mouse model is due to Lrig1+ keratinocyte stem cell expansion. J Invest Dermatol 2017;137:2208–16.

Lazarczyk M, Cassonnet P, Pons C, Jacob Y, Favre M. The EVER proteins as a natural barrier against papillomaviruses: a new insight into the pathogenesis of human papillomavirus infections. Microbiol Mol Biol Rev 2009;73:348–70.

Lechner M, Liu J, Masterson L, Fenton TR. HPV-associated oropharyngeal cancer: epidemiology, molecular biology and clinical management. Nat Rev Clin Oncol 2022;19:306–27.

Lei T, Du S, Peng Z, Chen L. Multifaceted regulation and functions of 53BP1 in NHEJ-mediated DSB repair [review]. Int J Mol Med 2022;50:90.

Mantovani A, Allavena P, Sica A, Balkwill F. Cancer-related inflammation. Nature 2008;454:436–44.

Marcuzzi GP, Hufbauer M, Kasper HU, Weißenborn SJ, Smola S, Pfister H. Spontaneous tumour development in human papillomavirus type 8 E6 transgenic mice and rapid induction by UV-light exposure and wounding. J Gen Virol 2009;90:2855–64.

Marthaler AM, Podgorska M, Feld P, Fingerle A, Knerr-Rupp K, Grässer F, et al. Identification of C/EBPα as a novel target of the HPV8 E6 protein regulating miR-203 in human keratinocytes. PLoS Pathog 2017;13:e1006406.

McBride AA. Human papillomaviruses: diversity, infection and host interactions. Nat Rev Microbiol 2022;20:95–108.

Michel A, Kopp-Schneider A, Zentgraf H, Gruber AD, de Villiers EM. E6/E7 expression of human papillomavirus type 20 (HPV-20) and HPV-27 influences proliferation and differentiation of the skin in UV-irradiated SKH-hr1 transgenic mice. J Virol 2006;80:11153–64.

Neagu M, Constantin C, Caruntu C, Dumitru C, Surcel M, Zurac S. Inflammation: a key process in skin tumorigenesis. Oncol Lett 2019;17:4068–84.

Olivero C, Lanfredini S, Borgogna C, Gariglio M, Patel GK. HPV-induced field cancerisation: transformation of adult tissue stem cell into cancer stem cell. Front Microbiol 2018;9:546.

Orth G. Genetics of epidermodysplasia verruciformis: insights into host defense against papillomaviruses. Semin Immunol 2006;18:362–74.

Pfister H. Chapter 8: human papillomavirus and skin cancer. J Natl Cancer Inst Monogr 2003;31:52–6.

Proby CM, Harwood CA, Neale RE, Green AC, Euvrard S, Naldi L, et al. A Case-Control Study of Betapapillomavirus infection and cutaneous squamous cell carcinoma in organ transplant recipients. Am J Transplant 2011;11:1498–508.

Quint KD, Genders RE, de Koning MNC, Borgogna C, Gariglio M, Bouwes Bavinck JN, et al. Human Beta-papillomavirus infection and keratinocyte carcinomas. J Pathol 2015;235:342–54.

Rahkola D, Laitala J, Siiskonen H, Pelkonen J, Harvima IT. Mast cells are a marked source for complement C3 products that associate with increased CD11b-positive cells in keratinocyte skin carcinomas. Cancer Invest 2019;37:73–84.

Ramoz N, Rueda LA, Bouadjar B, Montoya LS, Orth G, Favre M. Mutations in two adjacent novel genes are associated with epidermodysplasia verruciformis. Nat Genet 2002;32:579–81.

Rappold I, Iwabuchi K, Date T, Chen J. Tumor suppressor p53 binding protein 1 (53BP1) is involved in DNA damage-signaling pathways [published correction appears in J Cell Biol 2001;154:469. J Cell Biol 2001;153:613–20.

Ritter ML, Pirofski L. Mycophenolate mofetil: effects on cellular immune subsets, infectious complications, and antimicrobial activity. Transpl Infect Dis 2009;11:290–7.

Roberts MB, Fishman JA. Immunosuppressive agents and infectious risk in transplantation: managing the "Net State of immunosuppression". Clin Infect Dis 2021;73:e1302–17–e1317.

Rollison DE, Amorrortu RP, Zhao Y, Messina JL, Schell MJ, Fenske NA, et al. Cutaneous human papillomaviruses and the risk of keratinocyte carcinomas. Cancer Res 2021;81:4628–38.

Rollison DE, Viarisio D, Amorrortu RP, Gheit T, Tommasino M. An emerging issue in oncogenic virology: the role of beta human papillomavirus types in the development of cutaneous squamous cell carcinoma. J Virol 2019;93:e01003–18.

Saluzzo S, Pandey RV, Gail LM, Dingelmaier-Hovorka R, Kleissl L, Shaw L, et al. Delayed antiretroviral therapy in HIV-infected individuals leads to irreversible depletion of skin- and mucosa-resident memory T cells. Immunity 2021;54:2842–58.e5.

Schaper ID, Marcuzzi GP, Weissenborn SJ, Kasper HU, Dries V, Smyth N, et al. Development of skin tumors in mice transgenic for early genes of human papillomavirus type 8. Cancer Res 2005;65:1394–400.

Siebenhaar F, Metz M, Maurer M. Mast cells protect from skin tumor development and limit tumor growth during cutaneous de novo carcinogenesis in a Kit-dependent mouse model. Exp Dermatol 2014;23:159–64.

Simmonds M, Storey A. Identification of the regions of the HPV 5 E6 protein involved in Bak degradation and inhibition of apoptosis. Int J Cancer 2008;123:2260–6.

Smola S. Immunopathogenesis of HPV-associated cancers and prospects for immunotherapy. Viruses 2017;9:254.

Strickley JD, Messerschmidt JL, Awad ME, Li T, Hasegawa T, Ha DT, et al. Immunity to commensal papillomaviruses protects against skin cancer. Nature 2019;575:519–22.

Tampa M, Mitran CI, Mitran MI, Nicolae I, Dumitru A, Matei C, et al. The role of beta HPV types and HPV-associated inflammatory processes in cutaneous squamous cell carcinoma. J Immunol Res 2020;2020:5701639.

Tetzlaff MT, Curry JL, Ning J, Sagiv O, Kandl TL, Peng B, et al. Distinct biological types of ocular adnexal sebaceous carcinoma: HPV-driven and virus-negative tumors arise through nonoverlapping molecular-genetic alterations. Clin Cancer Res 2019;25:1280–90.

Tommasino M. The biology of beta human papillomaviruses. Virus Res 2017;231:128–38.

Tommasino M. HPV and skin carcinogenesis. Papillomavirus Res 2019;7:129–31.

Uitto J, Saeidian AH, Youssefian L, Saffarian Z, Casanova JL, Béziat V, et al. Recalcitrant warts, epidermodysplasia verruciformis, and the tree-man syndrome: phenotypic spectrum of cutaneous human papillomavirus infections at the intersection of genetic variability of viral and human genomes. J Invest Dermatol 2022;142:1265–9.

Underbrink MP, Howie HL, Bedard KM, Koop JI, Galloway DA. E6 proteins from multiple human Betapapillomavirus types degrade Bak and protect keratinocytes from apoptosis after UVB irradiation. J Virol 2008;82:10408–17.

Vahidnezhad H, Youssefian L, Saeidian AH, Mansoori B, Jazayeri A, Azizpour A, et al. A CIB1 splice-site founder mutation in families with typical epidermodysplasia Verruciformis. J Invest Dermatol 2019;139:1195–8.

Van Doorslaer K, Li Z, Xirasagar S, Maes P, Kaminsky D, Liou D, et al. The Papillomavirus Episteme: a major update to the papillomavirus sequence database. Nucleic Acids Res 2017;45:D499–506.

Vanharanta S, Massagué J. Field cancerization: something new under the sun. Cell 2012;149:1179–81.

Venuti A, Lohse S, Tommasino M, Smola S. Cross-talk of cutaneous beta human papillomaviruses and the immune system: determinants of disease penetrance. Phil Trans R Soc B Biol Sci 2019;374: 20180287.

Viarisio D, Mueller-Decker K, Kloz U, Aengeneyndt B, Kopp-Schneider A, Gröne HJ, et al. E6 and E7 from beta HPV38 cooperate with ultraviolet light in the development of actinic keratosis-like lesions and squamous cell carcinoma in mice [published correction appears in PloS Pathog 2016;12: e1006005] PLoS Pathog 2011;7:e1002125.

Viarisio D, Müller-Decker K, Accardi R, Robitaille A, Dürst M, Beer K, et al. Beta HPV38 oncoproteins act with a hit-and-run mechanism in ultraviolet radiation-induced skin carcinogenesis in mice. PLoS Pathog 2018;14: e1006783.

Wallace NA, Galloway DA. Manipulation of cellular DNA damage repair machinery facilitates propagation of human papillomaviruses. Semin Cancer Biol 2014;26:30–42.

Wallace NA, Robinson K, Howie HL, Galloway DA. HPV 5 and 8 E6 abrogate ATR activity resulting in increased persistence of UVB induced DNA damage. PLoS Pathog 2012;8:e1002807.

Wallace NA, Robinson K, Howie HL, Galloway DA. β-HPV 5 and 8 E6 disrupt homology dependent double strand break repair by attenuating BRCA1 and BRCA2 expression and foci formation. PLoS Pathog 2015;11:e1004687.

Weissenborn SJ, Nindl I, Purdie K, Harwood C, Proby C, Breuer J, et al. Human papillomavirus-DNA loads in actinic keratoses exceed those in non-melanoma skin cancers. J Invest Dermatol 2005;125:93–7.

Wendel SO, Wallace NA. Loss of genome fidelity: beta HPVs and the DNA damage response. Front Microbiol 2017;8:2250.

Willenbrink TJ, Ruiz ES, Cornejo CM, Schmults CD, Arron ST, Jambusaria-Pahlajani A. Field cancerization: definition, epidemiology, risk factors, and outcomes. J Am Acad Dermatol 2020;83:709–17.

Zavattaro E, Azzimonti B, Mondini M, De Andrea M, Borgogna C, Dell'Oste V, et al. Identification of defective Fas function and variation of the perforin gene in an epidermodysplasia verruciformis patient lacking EVER1 and EVER2 mutations. J Invest Dermatol 2008;128:732–5.

Zhao Y, Amorrortu RP, Fenske NA, Cherpelis B, Messina JL, Sondak VK, et al. Cutaneous viral infections associated with ultraviolet radiation exposure. Int J Cancer 2021;148:448–58.

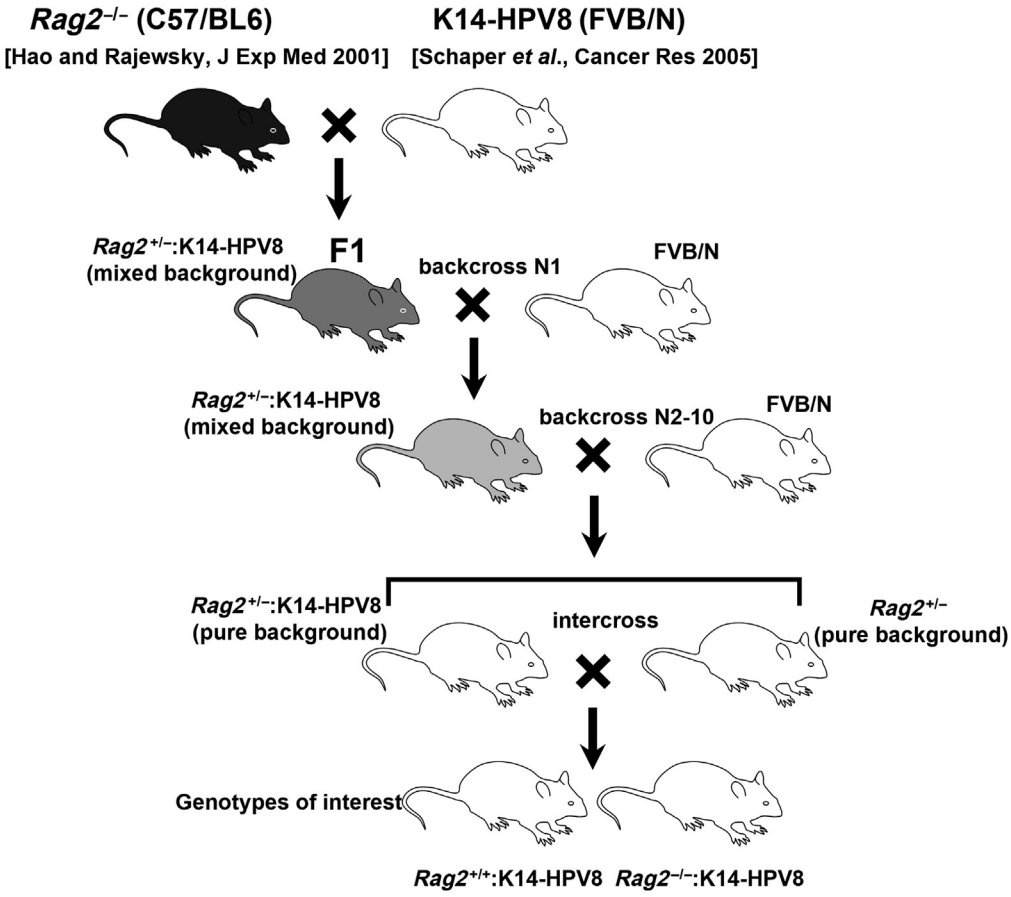

Supplementary Figure S1. Flowchart of the breeding procedure used to generate *Rag2*$^{-/-}$:K14-HPV8 mice. HPV, human papillomavirus.

Supplementary Figure S2. *Rag2*$^{-/-}$:K14-HPV8 mice aged 5 months showing lesions spreading to most of the skin surface, including the legs. HPV, human papillomavirus.

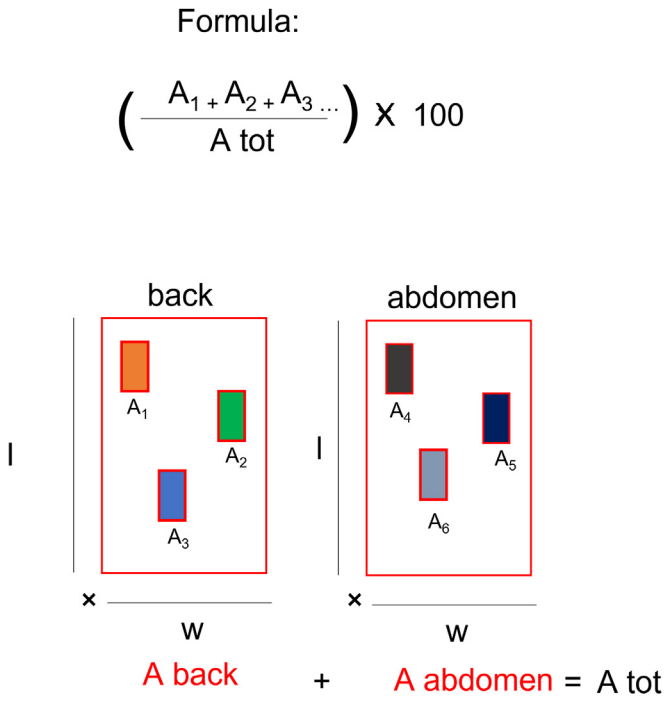

Supplementary Figure S3. Formula to calculate the percentage of the affected areas. A, area; $A_{1/2/3}$, area of the lesion; l, length; w, width.

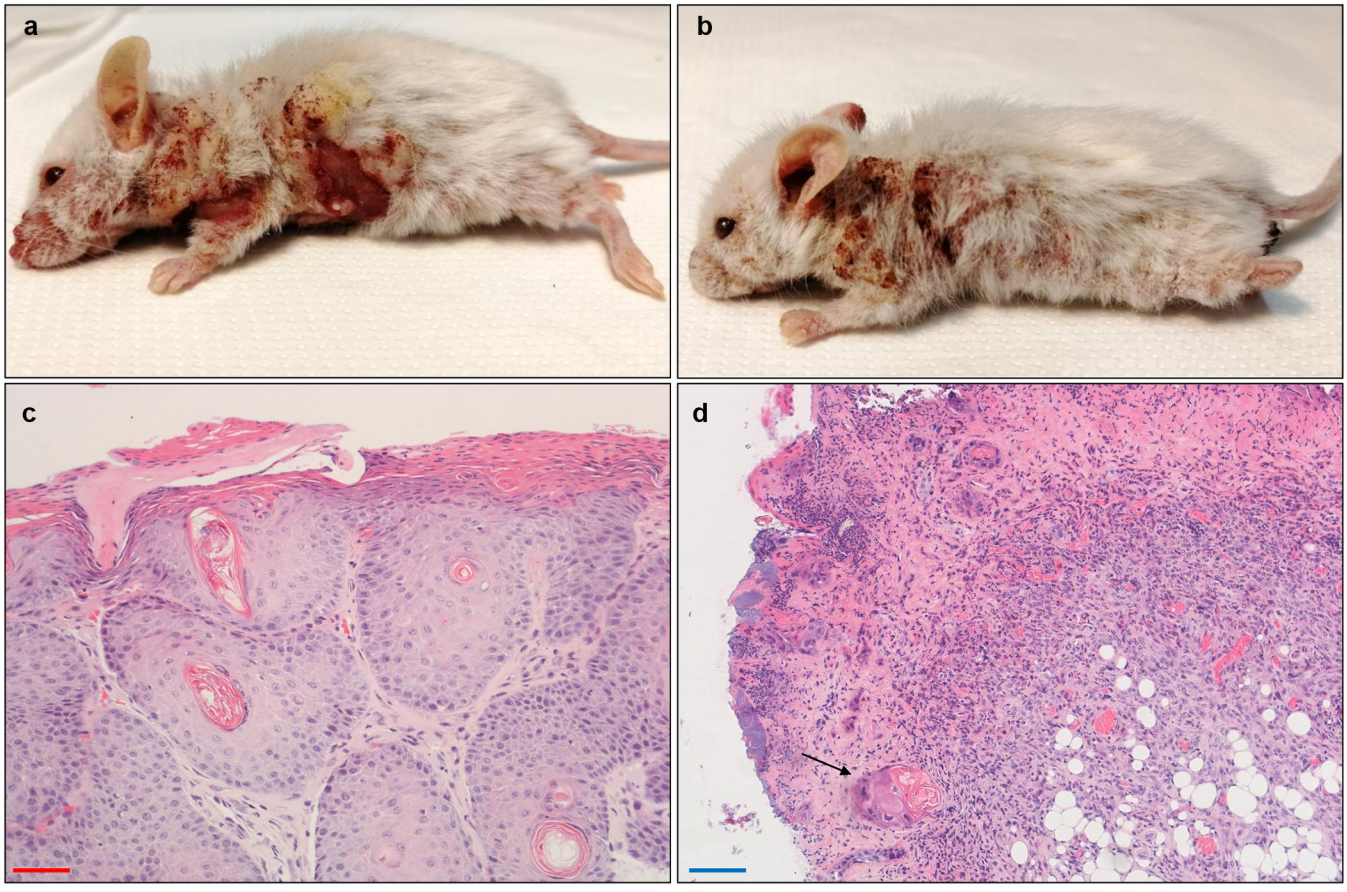

Supplementary Figure S4. *Rag2*$^{-/-}$:K14-HPV8 mice develop skin squamous cell carcinoma. (**a, b**) Representative pictures of the two *Rag2*$^{-/-}$:K14-HPV8 mice displaying skin squamous cell carcinoma. Panels **c** and **d** show the H&E images of the cutaneous lesions from the mouse of panel **a**. The tumors display well-differentiated areas with pearl-like structures surrounded by dermal nests of atypical keratinocytes (panel **c**) and ulcerated areas showing dysplastic foci (black arrow in panel **d**). Bar (red) = 50 μm; bar (blue) = 100 μm. HPV, human papillomavirus.

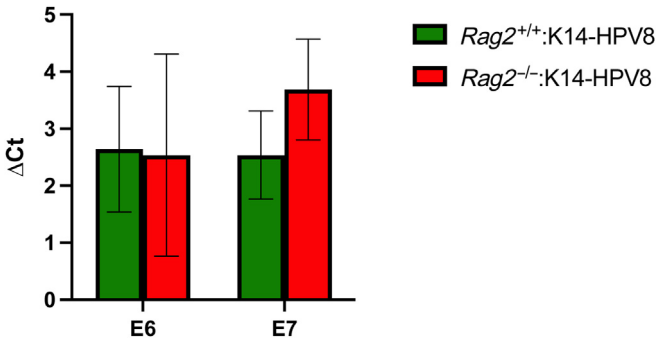

Supplementary Figure S5. HPV8 *E6* and *E7* transgenes are equally expressed in the lesional epidermis of the two HPV8-transgenic mice. RT-qPCR analysis of HPV8 *E6* and *E7* mRNA expression levels in lesional skin from *Rag2*$^{+/+}$:K14-HPV8 (green; n = 3) and *Rag2*$^{-/-}$:K14-HPV8 (red; n = 3). Values were normalized to mouse-specific β-actin and plotted as ΔCt. Data are represented as means ± SD. HPV, human papillomavirus.

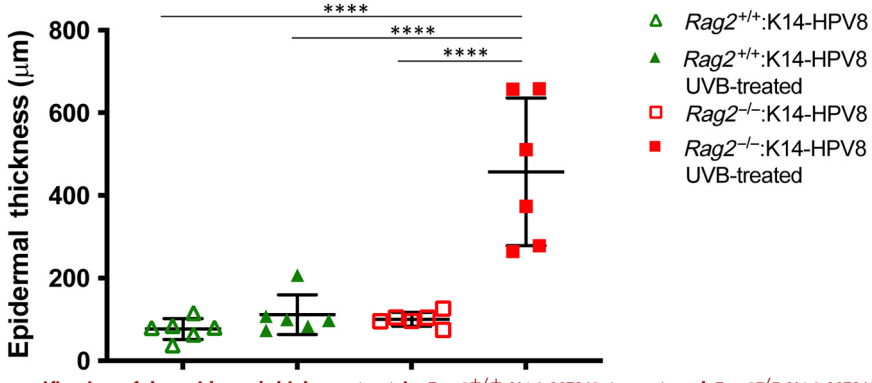

Supplementary Figure S6. Quantification of the epidermal thickness (μm) in *Rag2*$^{+/+}$:K14-HPV8 (green) and *Rag2*$^{-/-}$:K14-HPV8 (red) mice with or without UVB irradiation. Each symbol represents the mean value obtained by evaluating 10 tissue section areas from a single mouse (n = 6 for each genotype). Data are presented as mean ± SD. Statistical analysis was performed by classical one-way ANOVA followed by Tukey's post hoc test. ****$P < 0.0001$. All groups were compared, but only those that reached statistical significance are shown. HPV, human papillomavirus.

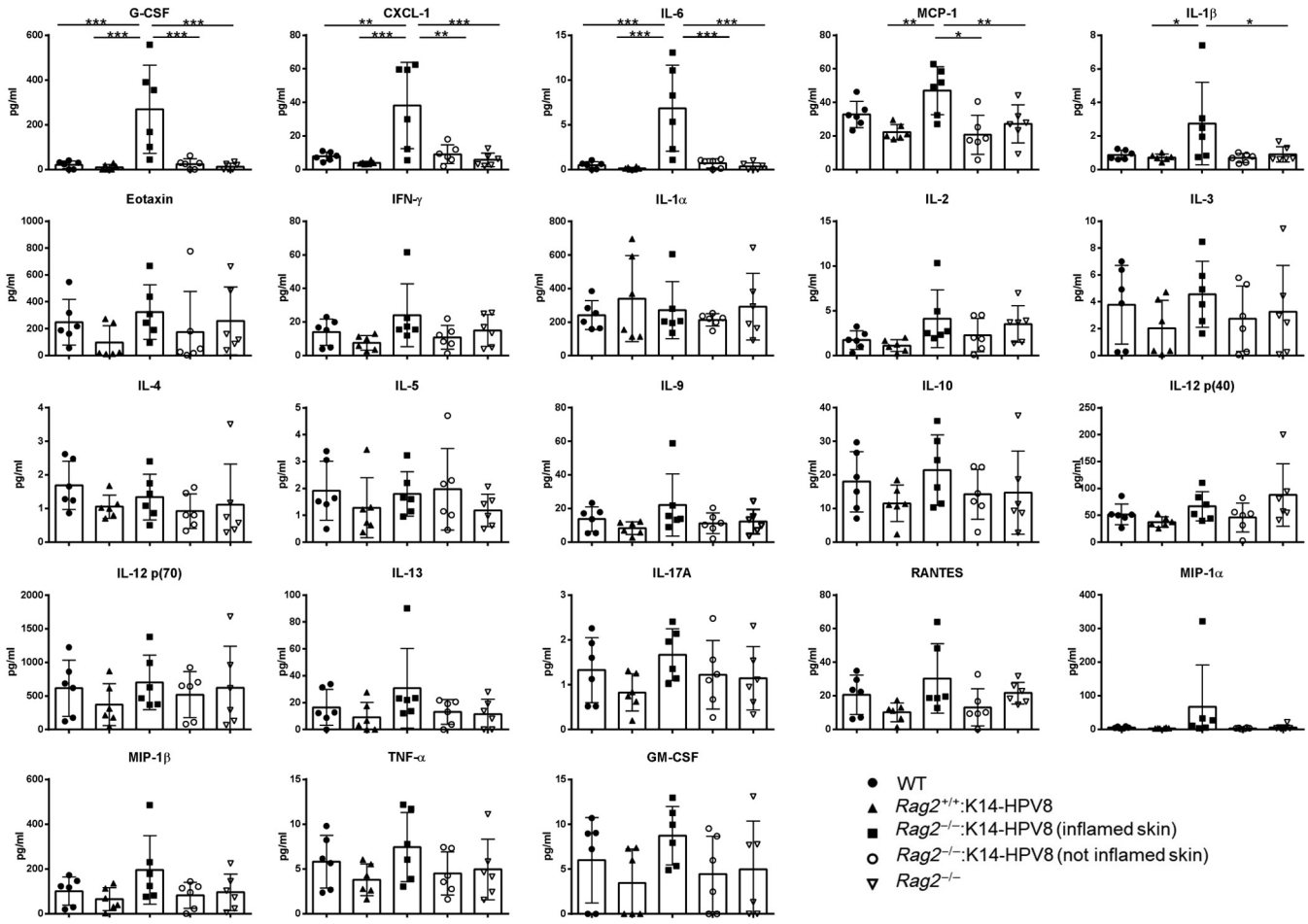

Supplementary Figure S7. Cytokine and chemokine profile in UVB-irradiated skin homogenates from WT, *Rag2*$^{+/+}$:K14-HPV8, *Rag2*$^{-/-}$:K14-HPV8 (inflamed or non-inflamed skin), and *Rag2*$^{-/-}$ mice using Bio-Plex Pro Mouse Cytokine 23-Plex Immunoassay. Each symbol represents the value of an individual mouse (n = 6 for each genotype). Data are represented as mean ± SD. Statistical analysis was performed by classical one-way ANOVA followed by Tukey's post hoc test. *$P < 0.05$, **$P < 0.01$, and ***$P < 0.001$. All groups were compared, but only those that reached statistical significance are shown. HPV, human papillomavirus; MCP-1, monocyte chemotactic protein-1; WT, wild type.